 CMES, vol.7, no.1, pp.1-17, 2005

An Effective Thermal-mechanical Modeling Methodology for Large-scale Area Array Typed Packages

H. C. Cheng[1], C. Y. Yu[2], and W. H. Chen[3]

Abstract: In this study, a simple but effective solution methodology that integrates a modified global/local finite element (GLFE) modeling technique and a two-staged constitutive modeling strategy is presented for the thermal-mechanical modeling of solder joints in an area array typed electronic package for characterizing the associated solder joint fatigue life under the JEDEC temperature cycling specification. The effectiveness and applicability of the proposed technique are demonstrated through two case studies, each of which is associated with an area array typed test vehicle. The geometry profile of solder joints in the test vehicle is determined by the Surface Evolver [Brakke (1996)]. For benchmark, a baseline finite element (FE) modeling is attempted by a conventional direct FE analysis (DFEA) approach. The DFEA approach employs a 3-D, fine-mesh FE model and a full constitutive law that takes both elastoplasticity and viscoelastic into account. The validity of the proposed thermal-mechanical modeling methodology is confirmed through existing experimental fatigue life data in literature as well as optical, interferometric measurement of the in-plane displacement field performed in this work. It turns out that the proposed methodology can efficiently and accurately deal with solder joint fatigue life prediction for large-scale area array typed electronic packages consisting of a large number of solder joints. In addition, results show that in terms of computational performance and solution accuracy, the methodology incorporating with the simplified constitutive law-Dwell Creep (DC) model could be a very ideal choice.

keyword: Global/local FE approach, Area array typed package, Fatigue life, Moiré interferometry.

[1] Associate Professor, Department of Aerospace and Systems Engineering, Feng Chia University, Taichung, Taiwan 407, R.O.C., hccheng@fcu.edu.tw

[2] Graduate Student, Department of Power Mechanical Engineering, National Tsing Hua University, Hsinchu, Taiwan 300, R.O.C.

[3] Professor, Department of Power Mechanical Engineering, National Tsing Hua University, Hsinchu, Taiwan 300, R.O.C., whchen@pme.nthu.edu.tw

1 Introduction

The low cycle fatigue has been well recognized as one of the leading failure mechanisms for solder joints subjected to temperature cycling loading. Many literatures demonstrated that by incorporating with a fatigue prediction model, such as the Coffin-Manson relationship, the fatigue life could be effectively characterized through a numerical approach [Pang, Seetoh and Wang (2000), Pang and Chong (2001), Akay, Liu and Rassaian (2003), Kaminishi, Iino, Bessho and Taneda (2000)]. For better prediction, this approach would generally require accurate and reliable stress/strain information. However, for large-scale area array typed electronic packages, a complex geometry, repetitive features and multi-materials/components are involved. One of the repetitive features can be considered as those hundreds up to thousands solder joints within the assembly. To precisely characterize the associated stress/strain information, three-dimensional (3-D) FE modeling with fine and high-quality mesh is generally required, which would lead to an impractical and prohibitive mesh count and result in an excessive computational time and cost. Basically, this concern could be relieved by creating a finer mesh at those suspicious solder joints while applying coarser mesh elsewhere, but unfortunately, the location of the most critical solder joint in reliability is generally unknown prior to modeling.

An alternative approach is the so-called global/local analysis technique. This scheme has been often applied in mechanical analysis of composite structures that comprise a consistent, repetitive materials pattern [see, e.g., Okada, Liu, Ninomiya, Fukui and Kumazawa (2004)]. The success of this approach is mainly dependent of a correct derivation of the effective properties of materials in the structures, and many mathematical models have been presented for the derivation, such as the

rule of mixture, the homogenization method [Sanchez-Palencia (1980), Guedes and Kikuchi (1990)], and the self-consistent method [Willis (1977)]. These techniques are unfortunately inapplicable for the current study since these solder joints are distributed in a discrete rather than continuous form. Later on, some researchers [see, e.g., Cobin (1993), Ju, Chan, Hareb and Lee (1995), Cheng, Chiang and Lee (1998)] proposed the FE-based global/local technique to deal with the problem. It is alternatively termed as the equivalent beam approach because these solder joints are thermal-mechanically modeled by an elastoplastic beam. The effective properties of the beam are derived through an iterative process that integrates the classical beam theory, FE modeling and a design of experiment (DOE) technique. In spite of its computational efficiency for modeling large-scale problems, certain, substantial drawbacks can still be observed, including a tedious derivation of the effective, elastoplastic properties and geometry constants of the equivalent beam and also lack of time-dependent creep model. It should be noted that these joints are commonly made of near eutectic solder alloy (63Sn/37Pb) due to its low melting temperature (T_m) and high service performance. It tends to undergo significant creep deformations when the operating temperature moves toward T_m; as a result, the creep behaviors would be essentially crucial to the long-term and low-cycle fatigue life of solder joints. Akay, Paydar and Bilgic (1997) pointed out that in predicting fatigue life of solder joints, the total strain energy criterion that accounts for all these three constitutive responses (elasticity, plasticity and creep) would have a much better prediction than that of the maximum strain range considering the creep effect only. In spite of that, simultaneously taking both plasticity and creep constitutive laws into account in the whole course of accelerated temperature cycling (ATC) test would require a significant computational effort, particularly when the number of solder joints is excessive.

To ease the difficulty, this study proposes a simple but effective solution methodology for simulating the thermal-mechanical behaviors of solder joints in an area array typed package under a JEDEC ATC test. The methodology incorporates a modified global/local FE modeling technique and a two-staged constitutive modeling strategy. Based on these derived stress/strain information together with the modified Coffin-Manson fatigue life prediction model [Engelmaier (1983)], the solder joint fatigue life is assessed. To confirm the effectiveness and applicability of the proposed approach, two area array typed packages, i.e., a 72 I/O and 225 I/O plastic ball grid array (PBGA) package, are considered as test vehicle. A baseline FE modeling associated with the 72 I/O test vehicle is performed for benchmark of the current methodology. Note that the baseline modeling employs a very fine 3-D FE model, a full constitutive law that accounts for both elastoplasticity and viscoelastic (alternatively termed as EPC or full constitutive model, as shown in Fig. 1(a)) to simulate the thermal-mechanical behaviors of solder joints, and a conventional DFEA approach in contrast to the currently proposed GLFE modeling technique. In addition, it is further noted that the geometry profile of the solder joint in the test vehicle is determined by the Surface Evolver [Brakke (1996)]. The validity of the FE modeling is confirmed through two manners: 1) optical, interferometric displacement measurement, i.e., moiré interferometry [see, e.g., Han and Guo (1995)], and 2) existing experimental solder joint fatigue life data [Mawer (1996)].

In the subsequent sections, the context of the paper is organized as follows. First of all, the proposed methodology is briefly introduced, and also, the FE modeling associated with the particular baseline modeling is constructed. Next, the validity of the baseline FE modeling and the current methodology are verified, and substantial results and discussions are made. Subsequently, another area array typed electronic package is performed to further substantiate the feasibility and effectiveness of the current technology. Finally, few essential concluding remarks are addressed.

2 The Proposed GLFE Modeling Technique

In the previous numerical studies of solder joint fatigue life, all the thermal-mechanical behaviors of those components in an electronic package are assumed linearly elastic, except solder joints. In general, solder would experience an elastoplastic deformation during temperature variation, and more importantly, it may also undergo a significant creep deformation even at room temperature. It has been extensively reported that the temperature-dependent and time-dependent inelastic strains are the major cause of the low-cycle fatigue of solder joints, and consequently, all these constitutive material behaviors, termed as the full constitutive law (EPC) in the study, should be taken into account in the thermal-mechanical

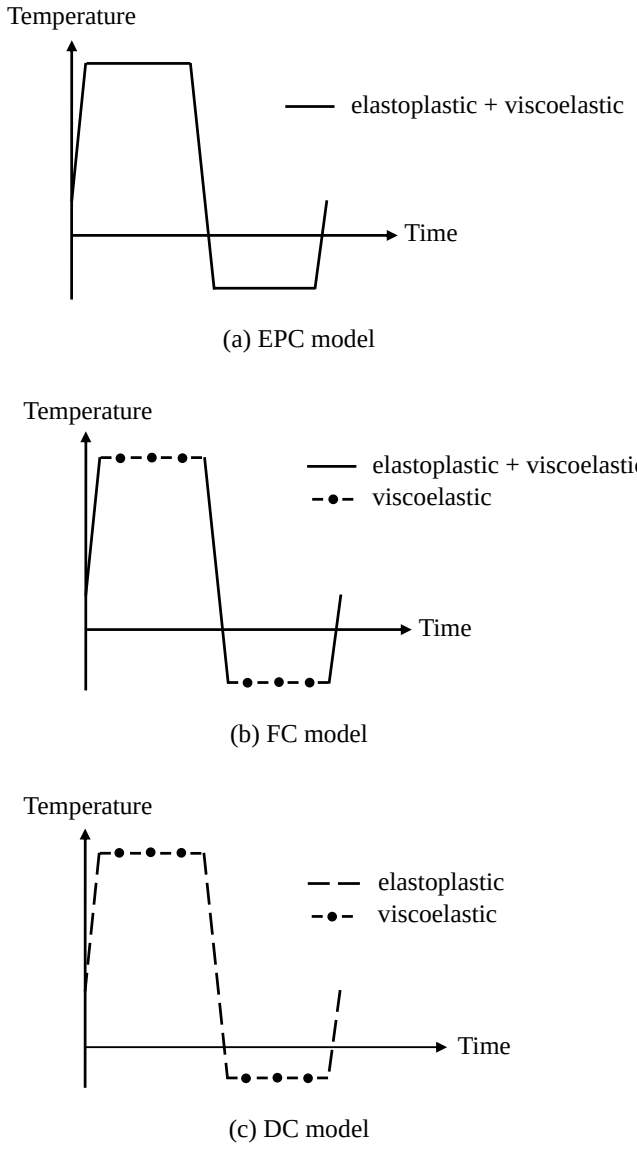

Figure 1 : Constitutive modeling strategies for solder joint

modeling of solder joints.

As mentioned earlier, applying the full constitutive law for the study of the electronic packages associated with a great deal of solder joints would, however, result in an impractical, computational expense. In literature, several simplified constitutive modeling strategies have been introduced, e.g., the Full Creep (FC) model [Pang, Seetoh and Wang (2000)], the Dwell Creep (DC) model [Pang, Seetoh and Wang (2000)] and the hybrid model [Cheng, Yu and Chen (2002)]. Both the FC and DC models, which are also shown in Fig. 1, acknowledge the significance of viscoelastic deformations during the temperature dwell periods of ATC loading while the plastic behavior is completely neglected in these periods. Furthermore, in addition to elastoplastic deformations, the FC model also allows solder joints undergoing creep deformations during the temperature-varying stages (i.e., temperature ramp-up/-down periods). This is, however, not allowed in the DC model. Pang, Seetoh and Wang (2000) indicated that although these two simplified strategies can yield an acceptable solution, the FC model provides a more accurate result than the DC model. This alternatively confirms that the creep deformations take place not only during the dwell time of ATC loading but also during the temperature ramp-up/-down stage. As a result, the FC model outperforms the DC model in solution accuracy. On the other hand, it was found that the computational efficiency of the DC model greatly surpasses that of the FC model. This leads to a modeling dilemma in how to efficiently model solder joint's thermal-mechanical behaviors while at the same time still maintaining good solution accuracy.

The currently proposed modeling methodology consists of two essential features. The first one is the proposal of a modified GLFE modeling approach to seize great computational efficiency. The other one is the integration of both the simplified and full constitutive modeling strategies in the analysis to pursue maximal computational efficiency while still maintain appropriate solution accuracy. It should be, however, noted that these two modeling strategies are not simultaneously involved in the analysis but instead, participated at a different analysis stage in the GLFE modeling approach and even at a different loading step in temperature cycling. The proposed GLFE modeling methodology can be briefed in the following. First of all, the global analysis employs a compact global FE model together with a simplified constitutive modeling strategy for effectively simulating the thermal-mechanical behaviors of solder joints. Basically, the objective of the global analysis is to explore the global thermal-mechanical behavior, i.e., deformation, of electronic packages during ATC test. A typical FE simulation makes use of the displacement-based approach, in which the displacement field would be C^0-continuity throughout the entire analysis domain, unlike stress/strain responses, which is C^1-continuity. This implies that the displacement field could be much less sen-

sitive to the mesh density in contrast to stress/strain responses, suggesting that a more compact mesh can be applied in the global analysis. To determine the mesh scale of the global model, a numerical experiment that employs a parametric FE analysis is conducted. By the compact global FE model, the computational effort can be greatly improved. Furthermore, it is also believed that creep strain would not have a great influence on the "global" displacement field of solder joints because creep generally takes place in the area of high-stressed zones, which are usually limited in some small, local regions. This makes creep become a very local phenomenon; consequently, it would have a very minor contribution to the overall deformation of solder joints. It is noted that, in general, the most critical-stressed zones in solder joints subjected to ATC loading usually locate nearby those four corners of solder joints adjacent to the upper/lower pads. This implies that it would not be vital for creep to fully get involved in the entire global analysis. By the above observation and presumption, a simplified constitutive model can be assumed in the global analysis. For comparison, both the DC and FC constitutive models are considered in the global FE modeling.

Once the most deformed solder joint is identified from the global analysis, its associated displacement field in the entire ATC itinerary is correspondingly extracted. Basically, the entire deformation history of the nodes in the global model that corresponds to the surface nodes of the local model should be completely extracted throughout the ATC loading. However, for computational simplification, the associated displacement field of these nodes is extracted only at those 26 checkpoints within the ATC duration, as shown in Fig. 2, and the deformation between two checkpoints is linearly interpreted using an interpolation scheme. Furthermore, these nodal displacement histories are interpreted and imposed on the surface nodes of the local model as an essential boundary condition for further local analysis using linear extrapolation and interpolation schemes. It should be further noted that the isothermal temperature loading that is applied in the global analysis is also used in the local analysis. By the displacement field, the local thermal-mechanical analysis of the particular solder joint subjected to the same ATC loading as the global analysis can be then performed to derive the associated comprehensive stress/strain responses. Basically, two main features can be observed in the local analysis. The first one is the application of a delicate local FE model with a fine mesh due to that stress/strain responses are very sensitive to the mesh density. In the investigation, a fine-meshed local model that consists of not only a solder joint but also a partial substrate and PCB due to the Saint Venant principle [Boresi and Chong (2000)] is used. Since the scale of the local model is trivial, as compared to the global model, the application of the fine-meshed local model would not deteriorate computational efficiency. The other is the incorporation of the full constitutive law in the local model in the entire ATC. Based on the calculated strain information, further prediction of the solder joint fatigue life is fulfilled using an empirical fatigue life prediction model.

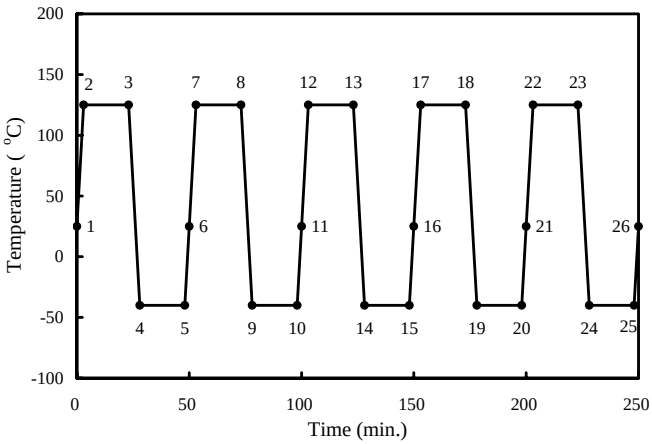

Figure 2 : Accelerated temperature cycling loading (JEDEC Test Method A105-B)

3 Finite Element (FE) Modeling

3.1 3-D FE models

To substantiate the effectiveness and feasibility of the current methodology, without loss of generality, two test vehicles are performed in the investigation. They are the 72 I/O and 225 I/O PBGA packages, as referred to the Motorola semiconductor technical report [Mawer (1996)]. A schematic diagram of a typical PBGA package is shown in Fig. 3.

In this study, the dimension of the package is 14×13 (*mm*), and the size of the embedded die is $6.86\times6.86\times0.36$ (*mm*). In the FE modeling, the geometry of the models is detailed enough to specify all

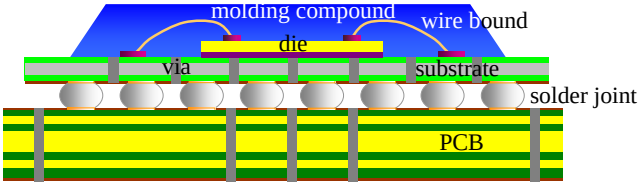

Figure 3 : The schematic diagram of a typical PBGA package

the main components of the test vehicles, including the molding compound, chip, substrate, PCB, and solder joints. The thickness of the molding compound, the substrate and the PCB is 0.36, 0.72 and 1.71 (*mm*), respectively. Geometry symmetry is used whenever possible to reduce the model size. In this aspect, only a quadrant of the package is included in the FE modeling for analysis with a symmetric boundary condition defined on the symmetry planes. In addition, to prevent the model from rigid body motion during FE analysis, the node at the bottom of the intersecting line of these two symmetry planes is rigidly constrained from the z-direction.

The geometry profile of the solder joints is calculated by using the Surface Evolver [Brakke (1996)], which is extensively applied in electronic packaging to estimate the shape of solder joints. Basically, a force balance system of a liquid solder joint is shown in Fig. 4.

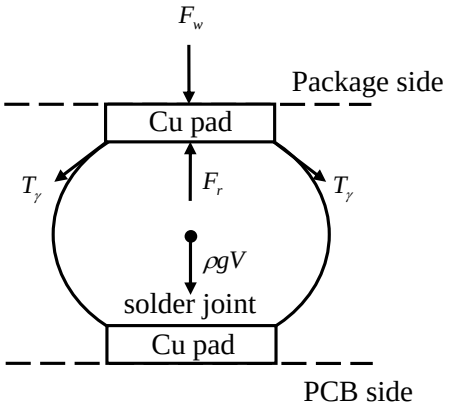

Figure 4 : A force balance system of a liquid solder joint

The total energy of a liquid solder joint is composed of the surface tension energy, the gravitation energy and the external energy. Based on these energies, the restoring force of solder joint can be written as:

$$F_r = \frac{\partial E}{\partial H} = \left(\frac{\partial E_{surface\_tension}}{\partial H} + \frac{\partial E_{gravity}}{\partial H} + \frac{\partial E_{external\_force}}{\partial H} \right) \quad (1)$$

where F_r is the restoring force, and E represents the total energy associated with standoff height of solder joint, H. Each part of the energy can be represented as:

$$\frac{\partial E_{surface\_tension}}{\partial H} = T_\gamma \iint_S \left(\nabla \cdot \vec{h} - \vec{n} \cdot D\vec{h} \cdot \vec{n} \right) dA \quad (2)$$

$$\frac{\partial E_{gravity}}{\partial H} = \rho g \iint_S \left[\nabla \cdot \left(\frac{z^2}{2} \vec{k} \right) \vec{h} - \nabla \times \left(\vec{h} \times \frac{z^2}{2} \vec{k} \right) \right] dA \quad (3)$$

$$\frac{\partial E_{external\_force}}{\partial H} = -P \frac{\partial V}{\partial H} = -P \iint_S \vec{h} \cdot d\vec{A} \quad (4)$$

where $\vec{h}$ is a variational vector and is equal to $\left[(z_{top} - z) / (z_{top} - z_{base} - H) \right] \vec{k}$, in which z_{top} and z_{base} represent the top and bottom boundary of solder joint, $\vec{n}$ is the outward unit normal vector of the surface, T_γ is the surface tension of the free surface S, ρ and g are the density and the acceleration of gravity, and $\vec{k}$ is the unit vector in the vertical direction. By imposing a downward or upward enforced deformation, the restoring force of solder joint along the vertical direction is then determined. When the downward force F_w induced from the weight of the package and the restoring force is balanced, the solder joint is in a force equilibrium condition, and then the shape of the solder joint could be estimated. Specifically, with a given solder joint volume (V) 0.268 mm^3, solder pad radius 0.381 *mm*, and a measured surface tension force 48.1 dynes/*mm*, the calculated standoff height H of the solder joint for the 72 I/O test vehicle is 0.463 *mm*. Furthermore, the 72 I/O PBGA package is chosen as a baseline model for benchmark of the current methodology. The baseline model employs a 3-D FE model with a very fine mesh, as shown in Fig. 5, in which it consists of 35,806 solid elements and 39,576 nodes.

3.2 *Constitutive Modeling*

The thermal-mechanical behaviors of components within the test vehicles are all considered linearly elastic except

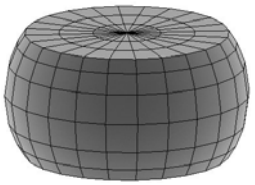

elements: 432
nodes: 511

(a) The FE model of a solder joint

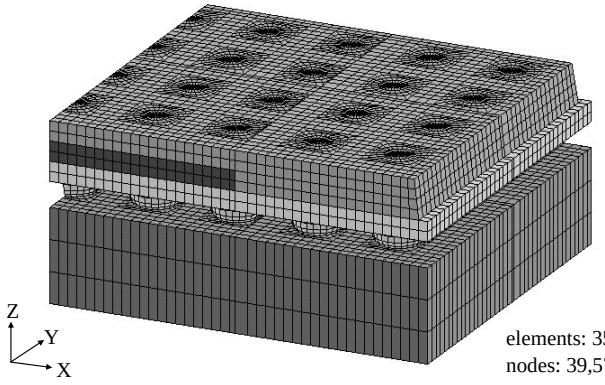

(b) The delicate FE model

Figure 5 : A quadrant of a delicate FE model for the 72 I/O PBGA package

those solder joints. Table 1 shows the material properties, originated from a Motorola semiconductor technical report [Mawer (1996)] and Zhang and Lee (1998). Note that the Prandtl-Reuss formulation [Chen and Han (1995)] is employed to simulate the temperature-dependent plasticity behavior for solder joints. The von Mises yield criteria, associated flow rule and kinematic hardening rule are employed to simulate the temperature-dependent plasticity behavior for solder joints. Fig. 6 shows the tensile stress-strain relationship of the eutectic solder based on Cheng, Chiang and Lee (1998). Furthermore, the constitutive equation that was presented in Lau (1995) and Lau and Pao (1997) to describe the time-dependent creep behavior of solder joints is also applied in the investigation, in which it is shown as follows:

$$\dot{\varepsilon}_{von}^{cr} = C_1 \sigma^{c_2} \exp(-Q/KT) \tag{5}$$

where $\dot{\varepsilon}_{von}^{cr}$ is the von Mises creep strain rate, σ_{von} the von Mises stress, T the absolute temperature, C_1 and C_2 correspond to the material constant and the stress exponent, respectively, Q is the activation energy and K is the Boltzamann constant. For a typical eutectic solder material, these constants can be defined as follows: $C_1 = 0.397\ \left(1/MPa^{C_2} \bullet mm\right)$, $C_2 = 5.25$, $Q = 0.49$(ev) and $K = 8.617\times10^{-5}$(ev/K) [Lau (1995), Lau and Pao (1997)].

Table 1 : The material properties of PBGA package

	E (GPa) (x,y/z)	Poisson ratio (xz, yz / xy)	CTE (ppm/^oC) (x,y/z)
Molding compound*	15.858	0.25	15
Chip*	130.31	0.278	2.6
Substrate*	15.17	0.195	13 / 57
PCB†	22 / 10	0.28 / 0.11	18 / 70

* Mawer (1996), † Zhang and Lee (1998)

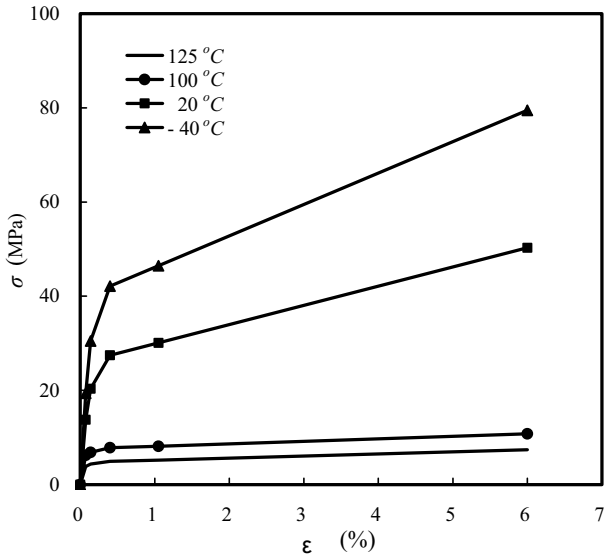

Figure 6 : The stress-strain curve of a typical eutectic solder

3.3 Accelerated Temperature Cycling (ATC) Loading

In the area of electronic packaging, the ATC test is the most typical one among those major environmental accelerated tests, and is generally applied for characterizing the associated solder joint reliability. It is usually performed in a more severe temperature loading environment together with a higher temperature cycling loading frequency. The current testing conforms to the JEDEC specification (JEDEC test method A105-B), and a typical ATC loading utilized in the investigation is shown

in Fig. 2. In the simulation, the ATC is considered as isothermal temperature loading. It comprises five major temperature loading/unloading steps with a total of 10-minute linear temperature ramp-up/-down and 40-minute low/high temperature dwell periods, and the temperature range of the ATC is from – 40^oC to 125^oC. Assume that the stress free condition is taken place at room temperature (25^oC). All the simulations in the investigation are conducted using the commercial FE code ANSYS® (Release 5.7).

3.4 Fatigue Life Prediction

In literature, many studies performed solder joint fatigue life prediction in electronic packaging using the modified Coffin-Manson correlation models [Engelmaier (1983), Solomn (1986), Mukai, Kawakami, Takahashi and Iwase (1997)]. Among them, the Engelmaier's model is by far one of the most popular Coffin-Manson correlation models. The model makes use of the total shear strain range to estimate the fatigue life of solder joints, and in addition, accounts for the effect of the temperature cycling frequency and temperature range. Accordingly, the modified, empirical, strain-based Coffin-Manson relationship applied herein is denoted as:

$$N_f = (1/2)\left(\Delta\gamma/2\varepsilon_f^{'}\right)^{1/c} \tag{6}$$

where N_f is the mean fatigue life or the mean cycle to failure, $\Delta\gamma$ is the total shear strain range in one temperature cycle, $\varepsilon_f^{'}$ is the fatigue ductility coefficient and is defined as 0.325, C is the fatigue ductility exponent and is equal to $-0.442-6\times10^{-4}T_{mean}+1.74\times10^{-2}\ln(1+f)$, T_{mean} represents the mean cycle solder joint temperature (^oC), which is equal to $1/2\,(T_{\max}+T_{\min})$, $T_{\max}$ and $T_{\min}$stand for the maximum cyclic temperature (^oC) and the minimum cyclic temperature (^oC), respectively, and f denotes the cyclic frequency (i.e., $1 < f < 1000$ cycles/day). Based on the von Mises yielding criterion, the relationship between the total shear strain γ and the von Mises strain ε_{von} can be expressed as below [Qian and Liu (1999), Pang and Chong (2001)]:

$$\gamma = \sqrt{3}\varepsilon_{von} \tag{7}$$

The von Mises strain ε_{von} is defined as follows:

$$\varepsilon_{von} = \frac{\sqrt{2}}{3}[(\varepsilon_x-\varepsilon_y)^2+(\varepsilon_y-\varepsilon_z)^2+(\varepsilon_z-\varepsilon_x)^2 + \frac{3}{2}(\gamma_{xy}^2+\gamma_{yz}^2+\gamma_{zx}^2)]^{1/2} \tag{8}$$

Accordingly, Eq. (6) can be rewritten as:

$$N_f = 1/2\left(\sqrt{3}\Delta\varepsilon_{von}/2\varepsilon_f^{'}\right)^{1/C} \tag{9}$$

where $\Delta\varepsilon_{von}$ is the cyclic von Mises strain range and is equal to $((\varepsilon_{von})_{\max}-(\varepsilon_{von})_{\min})$, in which $(\varepsilon_{von})_{\max}$ and $(\varepsilon_{von})_{\min}$ denote the maximum and minimum von Mises strain in a cycle, respectively. Once the cyclic von Mises strain range of the solder joint is derived, the associated solder joint fatigue life can be estimated based on the maximum cyclic von Mises strain range.

Since the temperature cycling of the experimental fatigue life data, which are from the Motorola semiconductor technical report [Mawer (1996)], is different from that of the current study, the predicted fatigue life of solder joints needs to be corrected by an acceleration factor before the comparison can be undertaken. This study takes advantage of the acceleration factor (AF) suggested by Lau (1995), which is approximately derived from an experimental test and is given as:

$$AF = N_{f(F)}/N_{f(L)}$$

$$AF = \left[\frac{\Delta T_F}{\Delta T_L}\right]^n\left[\frac{f_F}{f_L}\right]^{1/m}\exp\left[\frac{0.123}{K}\left(\frac{1}{(T_{\max})_F}-\frac{1}{(T_{\max})_L}\right)\right] \tag{10}$$

where the subscript L and F stand for those two different testing environments, ΔT is the maximum temperature range, K denotes the Boltzamann constant, and n and m correspond to -1.9 and 3, respectively, for an eutectic solder material.

4 Results and Discussions

4.1 Validation of the Baseline FE Modeling

Before the baseline model can be applied for benchmark of the proposed modeling methodology, its validity needs to be confirmed first. The thermal-mechanical simulation of the 72 I/O PBGA baseline model is first performed using the DFEA approach. Note that the simulation employs the full constitutive law (alternatively termed as the EPC model in this study) to model the solder material responses. It is also called the EPC-based DFEA approach. Correspondingly, the DFEA modeling that employs the FC or DC constitutive model is termed

as the FC- or DC-based DFEA approach, respectively. The calculated maximum cyclic von Mises strain range at the most deformed solder joint is 1.18%. Based on the Coffin-Manson fatigue life prediction model shown in Eq. (9), the associated solder joint fatigue life is found to be 2,353 cycles. For validation of the modeled fatigue life, the experimental data provided in the Motorola semiconductor technical report [Mawer (1996)] is applied. It showed that the solder joint fatigue life of the 72 I/O PBGA test vehicle subjected to a – 40^{o}C to 125^{o}C ATC loading with one hour per cycle is 2,171 cycles for 50% samples failure. Since the ATC loading frequency and also the loading time per cycle in the experiment are different from those of the current study, the modeled data is further modified by using an AF defined in Eq. (10). The determined AF is 1.06, and accordingly, the corrected, modeled fatigue life is 2,494 cycles for ATC in one hour per cycle. It turns out that there is only 15% difference in the predicted fatigue life of solder joints between the current EPC-based DFEA approach and the experiment. The agreement is considered fair. This demonstrates the appropriateness of the baseline FE model, and the associated baseline solution can be further applied to validate the current methodology.

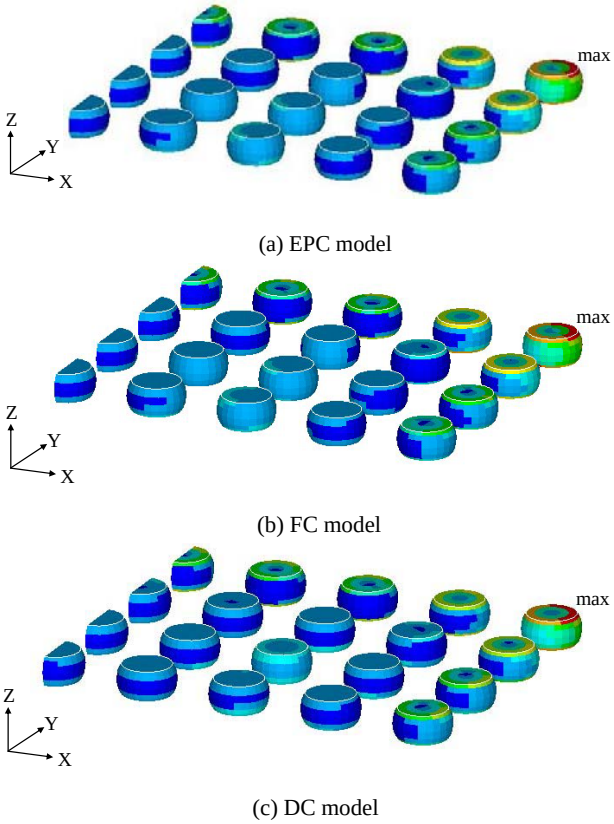

Figure 7 : The distribution of the von Mises strain (DFEA approach)

4.2 Solutions of the Direct FE Analysis (DFEA) Approaches

By comparing against the baseline modeling (EPC-based DFEA approach), the characteristics and feasibility of the DC- and FC-based DFEA approaches are investigated. It is particular to note that the location of the most critical solder joint in reliability or the most deformed solder joint is identical for all these three DFEA approaches. It is located at the outmost diagonal corner of the package (i.e., the maximum distance from the neutral point (the center of the package), DNP), as shown in Fig. 7. In addition, the associated maximum von Mises strains for these modelings are all located at the interface between the solder joint and the attached pad at the substrate side. This implies that the failure mechanism remains unchanged in these DFEA approaches.

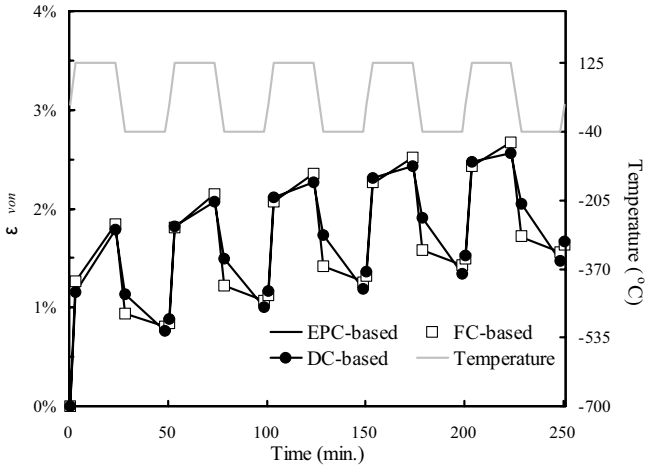

Figure 8 : The evolutionary history of von Mises strain (DFEA approach)

Fig. 8 shows the calculated von Mises strains associated with these three modeling approaches (i.e., the EPC-, FC- and DC-based DFEA). It is evident that a very good agreement is obtained between the EPC-based and FC-based DFEA approaches, suggesting that plasticity can be neglected in modeling solder joint's thermal-mechanical behaviors during the dwell periods of the ATC loading. In fact, this result is very similar to that

presented in Pang, Seetoh and Wang (2000). By further comparing the results of the DC-based with those of the EPC-based, a more distinct gap can be detected, particularly when the temperature drops from 125^{o}C to –40^{o}C and when the temperature is in the –40 ^{o}C dwell period (i.e., the checkpoints "3" to "5" during the first cycle, shown in Fig. 2). The maximum discrepancy can be as much as about 23%. This reveals the important role of creep not only at the temperature dwell periods but also at the temperature change. This fact was also observed in Pang, Seetoh and Wang (2000). On the other hand, it is also found in Fig. 9 that the discrepancy in the maximum von Mises strain between the DC-based and the EPC-based DFEA is only 4%. The minor difference implies that the neglect of creep modeling during the temperature variation stage would not deteriorate the solution accuracy in terms of the maximum von Mises strain, which generally occurs at the high temperature dwell period.

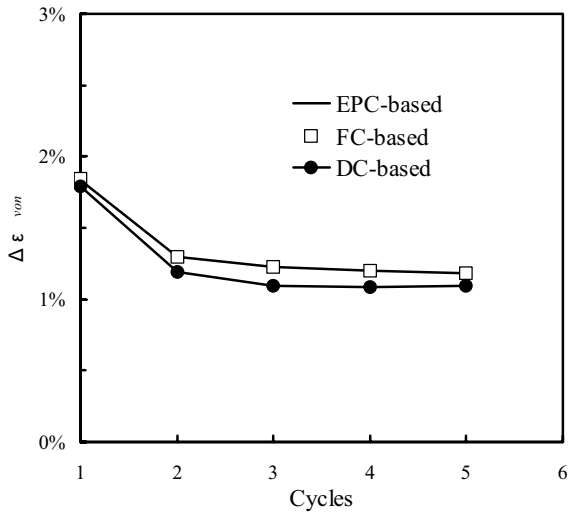

Figure 9 : The von Mises strain range versus temperature cycles (DFEA approach)

The associated von Mises strain ranges are illustrated in Fig. 9, with respect to the number of temperature cycles. The von Mises strain range obtained from the FC-based DFEA is almost identical to that of the EPC-based. This demonstrates the applicability of the FC constitutive model. On the other hand, the DC-based DFEA yields a larger discrepancy than the FC-based, and the difference is about 11%, which is still acceptable generally. The associated von Mises stresses are presented in Fig. 10, with respect to the number of temperature cycles. It is found that the FC-based DFEA approach, likewise, yields a very satisfactory solution accuracy in contrast to the baseline modeling, and in addition, there is a significant gap in the von Mises stress between the DC-based and the EPC-based DFEA approaches, particularly during the temperature changing from 125^{o}C to –40^{o}C and during the –40 ^{o}C dwell period.

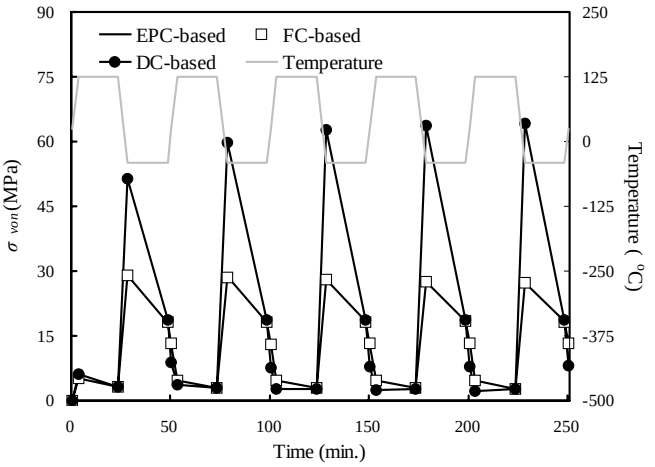

Figure 10 : The evolutionary history of von Mises stress (DFEA approach)

As much as about 136% difference is detected. This is also due to that creep was not taken into account in the modeling during the temperature variation periods of ATC loading; as a result, stresses in solder joints could not be relaxed by through solder creeping. Furthermore, Table 2 shows the required computational time of these three DFEA approaches. It is found that the computational cost of the FC-based and DC-based DFEA approaches is reduced up to 30% and 74%, respectively, as compared to that of the EPC-based approach. Despite that the degree of improvement through the FC-based DFEA approach is not extremely significant, the enhancement of the computational performance is still good. Nevertheless, as the number of I/Os continues increase in electronic packaging, the improvement can be more significant. Among these three constitutive models, the DC model provides better computational efficiency but poorer solution accuracy, particularly in the von Mises stress. However, it still provides an acceptable strain and strain range for using in the prediction of solder joint fatigue life. This may be the reason that the DC

Table 2 : Computational time for the 72 I/O PBGA package

Approach	Model	Computational time (sec.)
DFEA approach	EPC-based (Benchmark)	556,382 (100%)
	FC-based	390,179 (70.1%)
	DC-based	145,664 (26.2%)
GLFE approach	EPC-based	27,365 (4.9%)
	FC-based	25,183 (4.5%)
	DC-based (Present)	10,432 (1.9%)

model is still widely used for thermal-mechanical modeling of solder joint fatigue life [see, e.g., Pang, Seetoh and Wang (2000), Pang and Chong (2001)].

4.3 Solutions of the Proposed GLFE Modeling Technique

First of all, a very compact FE model is constructed for the global analysis. The mesh of the compact model is determined through a numerical experiment that employs a parametric FE analysis. The FE modeling utilizes the full constitutive model (EPC) to simulate the thermal-mechanical behaviors of solder joints. The determined compact model is shown in Fig. 11,

in which it consists of 6 layers of mesh in the thickness direction of solder joints, each of which comprises 16 solid elements. In addition, there is only one element in the thickness direction of the substrate and chip, and two elements for the PCB and the molding compound. In summary, it is composed of 4,466 elements and 5,182 nodes. As compared to the baseline FE model, a significant reduction of the mesh scale is made, implying that a great computational performance can be attained in the global analysis. By comparing the net deformation of the most deformed solder joint with that of the baseline modeling, there is only 0.55% discrepancy in the net in-plane deformation and 0.36% in the net out-of-plane deformation. In spite of such significant cut of the mesh scale, the compact model can still, as expected, provide an acceptable displacement field.

In the investigation, the DC, FC and EPC constitutive laws are, respectively, considered in the global analysis for comparison. The simulations associated with these three constitutive modeling strategies are simply termed as the DC-, FC- and EPC-based GLFE modeling, respectively. Five temperature cycles are performed in the global analysis. It will be confirmed later that five cycles are sufficient to derive a convergent strain. It should be noted that the solder joint undergoing the maximum net deformation happens to be the same one for these three simulations, which is also identical to that of the baseline solution. Furthermore, the associated displacement field of the most critical solder joint in the entire ATC testing is extracted, and is considered as the essential boundary condition of the local FE model for subsequent local

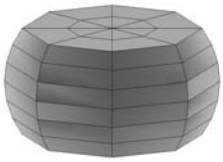

(a) The FE model of a solder joint in the compact global FE

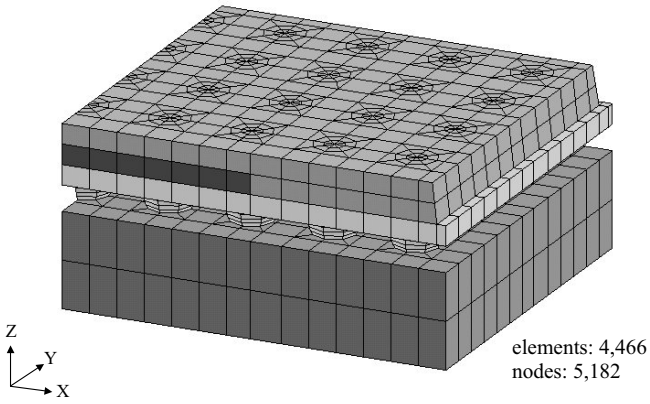

(b) A quadrant compact global FE model

Figure 11 : The compact global FE model for the 72 I/O PBGA package

analysis.

The local FE model for the investigation is presented in Fig. 12. It contains one third (in the thickness) of the PCB, a piece of the substrate and a solder joint. The total number of elements and nodes is 792 and 970, respectively. Note that for comparison purpose, the local FE model is exactly equivalent to the one used in the benchmarked model, and in addition, the full constitutive law is applied in the local analysis to thermal-mechanically model the solder joint. Fig. 13 presents the maximum von Mises strain associated with the DC-, FC-, and EPC-based GLFE modeling as well as the baseline modeling (i.e., the EPC-based DFEA approach) versus the number of temperature cycles.

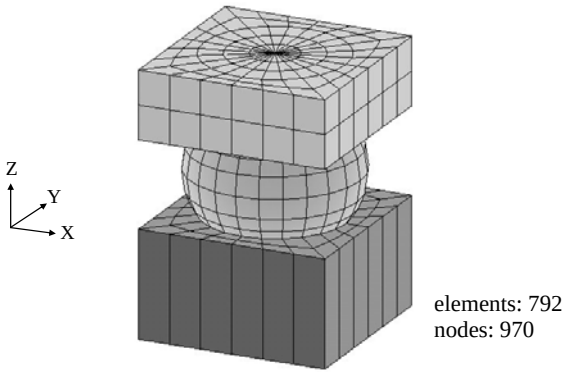

Figure 12 : The detailed local FE model for the most suspicious solder joint

It is found that, maximally, there is approximately 11% discrepancy in the von Mises strain between the baseline and EPC-based GLFE modeling, and also between that and the FC-based GLFE modeling, and 14% discrepancy between that and the DC-based GLFE modeling. These results again demonstrate the strength of the determined compact FE model and the effectiveness of the FC-based modeling. Likewise, the DC-based modeling presents a larger inaccuracy in von Mises strain in contrast to the FC-based modeling. However, the degree of inaccuracy (about 14%) is much smaller than that in the DFEA approach (about 23%).

The relation of the von Mises strain ranges versus the number of temperature cycles is shown in Fig. 14. It shows that the von Mises strain ranges obtained from both the DFEA and those three proposed GLFE modelings attain convergence after four temperature cycles.

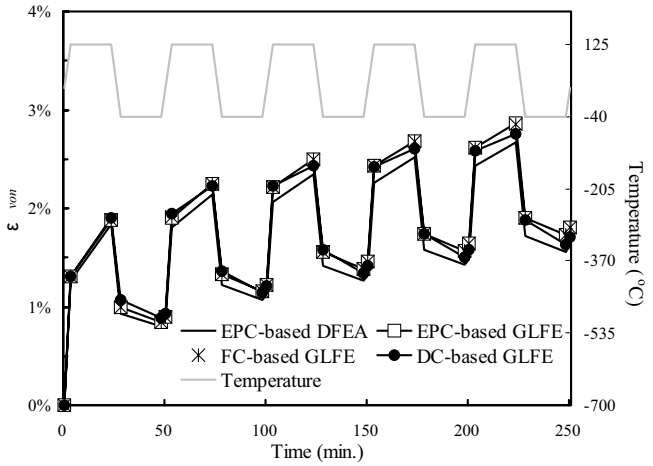

Figure 13 : The evolutionary history of von Mises strain (the proposed GLFE modeling technique)

In comparison with the baseline solution, the discrepancy in the von Mises strain range is about 3% at the 5^{th} cycle for both the EPC-based and FC-based GLFE modelings, and 0.2% for the DC-based GLFE modeling. It is not surprising to find again the applicability of the FC-based modeling approach. What surprises many is the trivial difference between the baseline and the DC-based modeling, as compared to their difference in the DFEA approach. In summary, regardless of the constitutive modeling strategy adopted, the currently proposed GLFE modeling technique can provide satisfactory solution accuracy. This confirms again the effectiveness of the current technique. The associated von Mises stresses are also shown in Fig. 15, versus the number of temperature cycles. It can be observed in the figure that the difference between the current GLFE technique that employs either the FC or DC constitutive law and the baseline modeling is under 13% only. Moreover, it is also surprising to find that the difference in the maximum von Mises stress by the DC constitutive law is only about 2%. The degree of inaccuracy is significantly less than that of the DFEA approach that adopts the DC constitutive law (136% difference, as shown in Fig. 10).

The associated computational effort is shown in Table 2. As can be found in the table, the EPC-, FC- and DC-based GLFE modelings take only about 4.9%, 6.5% and 7.2% computational time, respectively, of the DFEA approach. In contrast to the baseline modeling, 20 (i.e., the EPC-based) to 50 (i.e., the DC-based) times of computa-

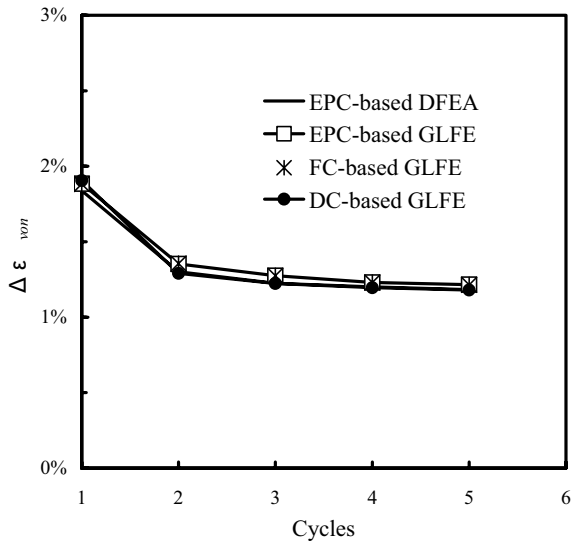

Figure 14 : The von Mises strain range versus temperature cycles (the proposed GLFE modeling technique)

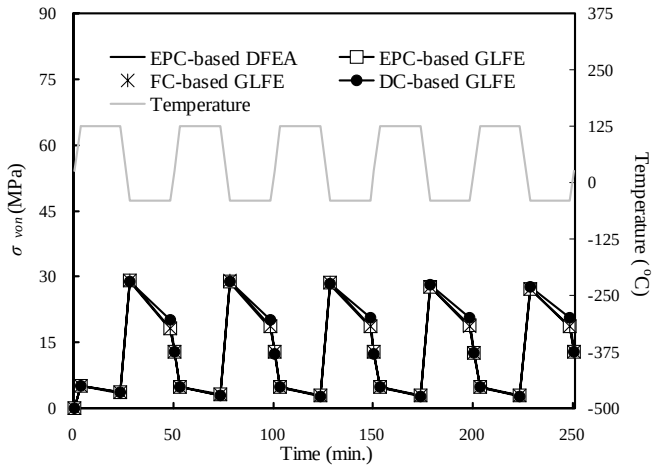

Figure 15 : The evolutionary history of von Mises stress (the proposed GLFE modeling technique)

tional performance are achieved by the current technique. Furthermore, it is also found that regardless of the DFEA or GLFE modeling, the computational performance of the DC-based modeling can be 2.5 times better than that of the FC-based. In brief, the modified GLFE modeling technique significantly outperforms the DFEA approach in terms of computational efficiency, and moreover, the computational performance of the DC-based modeling is also much superior to that of the FC-based.

From the above results, it is concluded that the DC-based GLFE modeling technique can be a very ideal choice for use in the thermal-mechanical modeling of solder joints due to its great computational performance and adequate solution accuracy.

4.4 Solder Joint Fatigue Life Prediction

Even though the accuracy of the von Mises strain, stain range, and stress obtained from the DFEA and the modified GLFE modeling techniques has been extensively demonstrated and compared in the previous sections, their effect on the solder joint fatigue life is still unknown yet due to that there presents no linear relationship between strain and fatigue life. Thus, the computed strain ranges are further applied in the Coffin-Manson relationship shown in Eq. (9) and (10) to predict the solder joint fatigue life of the 72 I/O PBGA. The estimated fatigue life is shown in Table 3. It is found that the fatigue life obtained from the FC-based DFEA approach is exactly the same as that of the baseline model. In other words, the difference between the FC-based DFEA approach and the experimental data remains about 15%, as mentioned in section 4.1, which is equivalent to that made by the baseline modeling. In addition, there is about 40% difference in the solder joint fatigue life prediction made by the DC-based DFEA approach. The results again reveal the advantage in the employment of the FC constitutive law in the DFEA approach, which has also been pointed out by Pang, Seetoh and Wang (2000).

Furthermore, the solder joint fatigue life predicted by the current technique associated with the EPC, FC and DC constitutive models for solder joints is, respectively, 2,317, 2,327 and 2,494 cycles. In comparison with the experimental fatigue life data, the associated difference is 6.7%, 7.2% and 14.9%. The prediction is good even for the DC-based GLFE modeling approach, which in fact could not be found in the DFEA approach. Furthermore, by comparing them with those of the DFEA approach, there is indeed a noticeable inconsistency. This could be due to that the empirical, strain-based fatigue life prediction model- the Coffin-Manson relationship, as shown in Eq. (6), consists of a negative exponent (i.e., about -2); as a result, a small perturbation in the calculated von Mises strain range would create a substantial difference in the predicted fatigue life. As mentioned earlier, the difference in the von Mises strain range associated with these three GLFE modelings (EPC-, FC- and DC-) when comparing with the baseline solution (i.e., the EPC-based

Table 3 : Fatigue life prediction of solder joints for the 72 I/O PBGA package

Approach	Model	Fatigue life (cycles)	Difference (%)
Experiment*		2,171	-
DFEA approach	EPC-based (Benchmark)	2,494	14.9
	FC-based	2,494	14.9
	DC-based	3,027	39.4
GLFE approach	EPC-based	2,317	6.7
	FC-based	2,327	7.2
	DC-based (Present)	2,494	14.9

* Mawer (1996)

DFEA) is quite inconsequential, in which there is only about 3% for the EPC-based and FC-based GLFE, and 0.2% for the DC-based GLFE. As further compared with those of the DFEA approach, the difference is only 3% in the EPC-based modeling, 3% also in the FC-based modeling and about 8% in the DC-based modeling. The discrepancy is also inconspicuous, implying that a fairly consistent result is obtained from these two approaches.

4.5 The Second Application

In order to further demonstrate the effectiveness and applicability of the current methodology, a typical PBGA containing 225 solder joints, which can be also referred to the Motorola semiconductor technical report [Mawer (1996)], is considered as the second test vehicle. The geometry of the PBGA package and the size of the embedded die is 27×27 (*mm*) and $10.16\times10.16\times0.36$ (*mm*), respectively. The thickness of the molding compound, the substrate and the PCB is 0.97, 0.36 and 1.71 (*mm*), respectively. Likewise, due to the symmetry of the package, only a quadrant of the package is modeled in the FE analysis. The standoff height and geometry profile of solder joints are determined through the Surface Evolver [Brakke (1996)]. The standoff height is 0.51 *mm* with a given solder joint volume, 0.268 mm^3, solder pad radius, 0.35 *mm*, and a measured surface tension force, 48.1 dynes/*mm*. In spite of the use of a quadrant symmetry condition, there are still about 56 solder joints in the FE model. This would result in a great scale of mesh, and eventually lead to excessive computational time when performed by using the DFEA approach. Hence, the model can be very ideal for use in verification of the feasibility and effectiveness of the current technique. The associated compact global FE model is constructed, as shown in Fig. 16. The model comprises 14,508 solid elements and 16,895 nodes. It should be noted that there is no baseline modeling for the current test vehicle due to the requirement of uncountable computational time for detailed modeling of the test vehicle.

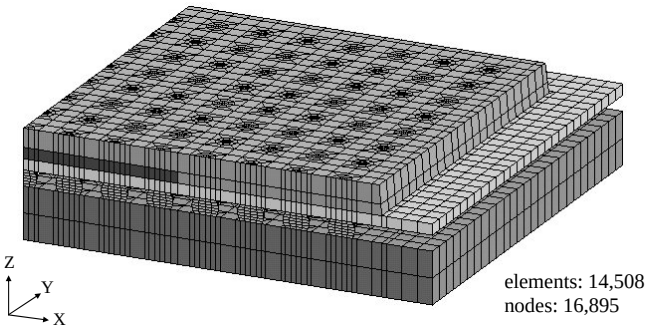

Figure 16 : The compact global FE model (225 I/O PBGA package)

The fatigue life obtained from the current technique is directly compared against the experimental data (Motorola

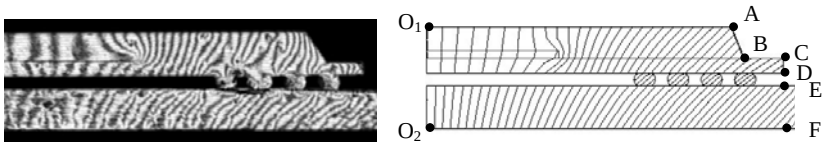

(a) U-field

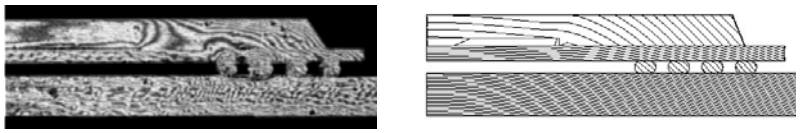

(b) V-field

Figure 17 : Simulated and experimental results of 256 PBGA package corresponding to the isothermal loading from 100^{o}C to 25^{o}C

Table 4 : Comparison between the experimental and simulated results

	Relative displacement (μm)				Difference (%)	
	Experiment		FEA			
	U-field	V-field	U-field	V-field	U-field	V-field
A	10.50	6.22	10.80	5.94	2.9	4.5
B	11.75	4.97	12.61	5.16	7.3	3.8
C	14.26	6.63	14.18	7.57	0.6	14.2
D	14.47	5.80	15.04	5.15	3.9	11.2
E	15.01	-	16.78	19.32	11.8	-
F	16.26	-	18.85	10.88	15.9	-

semiconductor data [Mawer (1996)]). In addition, the validity of the current technique for stress/strain characterizations is confirmed by the EPC-based GLFE modeling. Alternatively, the feasibility of the global FE modeling for exploring the displacement field is also examined through the moiré interferometric measurement. In the measurement, a virtual reference grating frequency with a frequency of 2400 lines/*mm*, which corresponds to a sensitivity of 0.417 μm/fringe, is utilized. The specimen is subjected to an isothermal swing loading in which the temperature drops from 100^{o}C to 25^{o}C. The measured displacement field associated with a right half of the PBGA is depicted in Fig. 17. Point A – F, illustrated in Fig. 17, are selected for comparison. O_1 is the reference point to point A – D, and O_2 is the reference point to point E – F. As can be observed in Fig. 17, the fringe in the V-field at the PCB is too dense to be counted. Consequently, the V-field relative displacements at point E – F are not taken into account in the validation. The U-field and V-field relative displacements at these points are shown in Table 4, associated with the measurement and the FE modeling. By comparing the modeled and measured results, it is found that there is less than 16% and 14% difference in the U-field and V-field relative displacements, respectively, at point A – F. The discrepancy can be considered insubstantial.

The linear material properties associated with the components in the test vehicle are also shown in Table 1, and the temperature-dependent stress/strain relationship and time-dependent creep behavior of solder material are also, respectively, presented in Fig. 6 and Eq. (5). The applied local FE model for the local analysis is equivalent to that used in the 72 I/O PBGA test vehicle. The applied ATC loading is also identical to the one used in the previous practice, shown in Fig. 2. It has been extensively confirmed in the previous discussions that the DC-based GLFE modeling technique can provide adequate solution accuracy and very good computational performance. Thus, the DC-based GLFE modeling technique is employed in the investigation. In addition, the EPC-

based GLFE modeling approach is also applied for comparison.

In the Motorola semiconductor data [Mawer (1996)], the test vehicle subjects to an ATC test under a temperature cycling loading with a temperature range of $0^oC \sim 100^oC$ and with the loading frequency of two cycles per hour. The stress free condition is also room temperature (25^oC). Their experimental data show that the associated solder joint fatigue life is 7,737 cycles for 50% sample failure.

In the numerical simulation, there is 14% difference in the von Mises strain and 18% difference in the von Mises stress between the EPC-based and DC-based GLFE modeling techniques. Fig. 18 demonstrates the calculated von Mises strain ranges associated with these two modeling approaches. It is found that the maximum von Mises strain range is 1.18E-2 and 1.13E-2 at the 5^{th} cycle, corresponding to the EPC-based and DC-based modeling techniques. Their difference is only about 4.2%. The degree of difference is very similar to that of the 72 I/O PBGA design, which is 3.3%, as shown in Fig. 14. Based on the modified Coffin-Manson relationship shown in Eq. (9), the fatigue life predicted by the DC-based and EPC-based is 2,616 and 2,353 cycles, respectively. The discrepancy is only 11%.

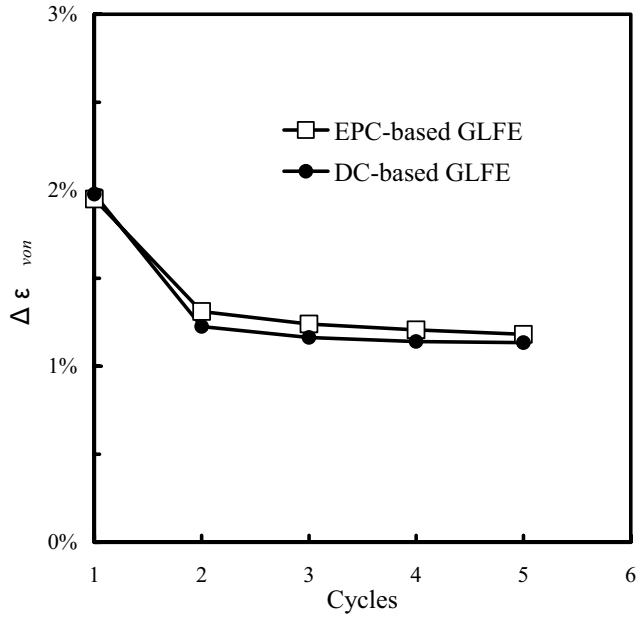

Figure 18 : von Mises strain range (225 I/O PBGA package

Since the temperature range and loading frequency in the experimental test are also different from those of the current simulations, the simulated fatigue life needs to be correspondingly adjusted through an AF. The calculated AF based on Eq. (10) is 3.9. By the AF, the modeled fatigue lives are, respectively, transformed into 10,202 and 9,177 cycles by the DC-based and EPC-based. As compared to the experimental fatigue life, the difference is about 19% between the EPC-based GLFE modeling and the experiment, and about 32% between the DC-based GLFE modeling and the experiment. Even though there is considerable 32% difference, which is still regarded as sufficient accuracy for predicting the fatigue life of electronic packaging. The gap between the EPC-based and DC-based modeling is only 13%, which is very similar to that of the 72 I/O PBGA assembly with about 8.2%. This implies that once the solution accuracy of the numerical modeling is upgraded, through, e.g., extensive characterization of actual material properties and also the coefficients of the acceleration factor presented in Eq. (10), the results of the DC-based GLFE modeling technique could be accordingly enhanced.

5 Conclusion

This study proposes a simple but effective thermal-mechanical solution methodology for the characterization of thermal-mechanical behaviors of solder joints in large-scale area array typed electronic packages subjected to a JEDEC temperature cycling test. Through two analysis practices using two area array typed PBGA packages, the effectiveness and applicability of the current methodology are extensively confirmed through an experimental data of the fatigue life, the baseline solution (i.e., the EPC-based DFEA approach) of the stress/strain responses, and alternatively, moiré interferometry measurement of the in-plane deformations. It turns out that the current approach can make the complex, thermal-mechanical modeling of large-scale area array typed electronic packages feasible and efficient.

From the obtained results, few concluding remarks are underlined:

a)Good correlation between the experimental data and the baseline results is obtained, demonstrating the effectiveness of the currently proposed methodology.

b)The FC constitutive modeling strategy provides better solution accuracy than the DC model, implying that

creep response during temperature ramp-up/-down periods would play a certain role in solder joint fatigue life.

c)By the currently proposed GLFE solution approach, even the most simplified DC-based constitutive modeling can provide fair solution accuracy in von Mises strain range, which is applied in Eq. (9) for further solder joint fatigue life prediction, and also von Mises stress. Furthermore, it is evident that the minimum computational effort is achieved by the DC-based GLFE modeling technique. It takes only about 2% of that of the EPC-based DFEA modeling technique, and even for the GLFE approach, only 38% of the computational time of the EPC-based GLFE is required.

d)Through the second numerical practice, the feasibility of the current methodology is demonstrated again.

Despite that the FC-based modeling could provide a more accurate result than the DC-based approach, the DC-based GLFE modeling technique would be considerably ideal particularly when the modeling scale is excessive based on its excellent computational performance and adequate solution accuracy.

Acknowledgement: The authors are grateful to the National Science Council, Taiwan, R.O.C., for partial financial support of the research under grants NSC-90-2212-E-007-055 and NSC-90-2212-E035-022. The help from Prof. W.C. Wang, Mr. Shao and Mr. Young for conducting the moiré interferometric measurements is deeply appreciated.

References

Akay, H. U.; Liu, Y.; Rassaian, M. (2003): Simplification of finite element models for thermal fatigue life prediction of PBGA packages. *Journal of Electronic Packaging*, vol. 125, pp. 347-353.

Akay, H. U.; Paydar, N. H.; Bilgic, A. (1997): Fatigue life predictions for thermally loaded solder joints using a volume-weighted averaging technique. *Journal of Electronic Packaging*, vol. 119, pp. 228-235.

Brakke, K. A. (1996): Surface evolver manual. Geometry center, University of Minnesota at Minneapolis St. Paul.

Boresi, A. P.; Chong, K. P. (2000): Elasticity in engineering mechanics, John Wiley & Sons, Inc.

Chen, W. F.; Han, D.J. (1995): Plasticity for structural engineers, Gau Lih Book CO., Ltd.

Cheng, H. C.; Chiang, K. N.; Lee, M. H. (1998): An effective approach for three-dimensional finite element analysis of ball grid array typed packages. *Journal of Electronic Packaging*, vol. 120, pp. 129-134.

Cheng, H. C.; Yu, C. Y.; Chen, W. H. (2002): Effective thermal-mechanical modeling of solder joints. *2002 ASME International Mechanical Engineering Congress & Exposition*, vol. 2.

Cobin, J. S. (1993): Finite element analysis for SBC structural design optimization. *IBM Journal of Research and Development*, vol. 37, pp. 585-589.

Engelmaier, W. (1983): Fatigue life of leadless chip carrier solder joints during power cycling. *IEEE Transactions on Components, Hybrids, and Manufacturing Technology*, pp. 232-237.

Guedes, J. M.; Kikuchi, N. (1990): Preprocessing and postprocessing for materials based on the homogenization method with adaptive finite element methods. *Computer Methods in Applied Mechanics and Engineering*, vol. 83, pp. 143-198.

Ham, S. J.; Lee, S. B. (2003): Measurement of creep and relaxation behaviors of wafer-level CSP assembly using moiré interferometry. *Journal of Electronic Packaging*, vol. 125, pp. 282-288.

Han, B.; Guo, Y. (1995): Thermal deformation analysis of various electronic packaging products by moiré and microscopic moiré interferometry. *Journal of Electronic Packaging*, vol. 117, pp. 185-191.

Ju, T. H.; Chan, Y. W.; Hareb, S. A.; Lee, Y. C. (1995): An integrated model for ball grid array solder joint reliability. *Structural Analysis in Microelectronic and Fiber Optic Systems*, EEP-Vol. 12, pp. 143-198.

Kaminishi, K.; Iino, M.; Bessho, H.; Taneda M. (2000): Numerical simulation of fatigue crack growth in microelectronics solder joints. *CMES: Computer Modeling in Engineering & Sciences*, vol. 1, no. 1, pp. 107-110.

Lau, J. H. (1995): Ball grid array technology, McGraw-Hill, Inc.

Lau, J. H.; Pao, Y. H. (1997): Solder joint reliability of BGA, CSP, flip chip, and fine pitch SMT assemblies, McGraw-Hill, Inc.

Mawer, A. (1996): Plastic ball grid array (PBGA). Motorola semiconductor technical data (AN1231/D).

Mukai, M.; Kawakami, T.; Takahashi, K.; Iwase, N. (1997): Thermal fatigue life predication of solder using stress analysis. *IEMT/IMC Proceedings*, pp. 204-208.

Okada, H; Liu, C. T.; Ninomiya T.; Fukui, Y.; Kumazawa, N. (2004): Analysis of particulate composite materials using an element overlay technique, *CMES: Computer Modeling in Engineering & Sciences*, vol. 6, no. 4, pp. 333-348.

Pang, J. H. L.; Chong, D. Y. R. (2001): Flip chip on board solder joint reliability analysis using 2-D and 3-D FEA models. *Advanced Packaging*, vol. 24, pp. 499-506.

Pang, J. H. L.; Seetoh, C. W.; Wang, Z. P. (2000): CBGA solder joint reliability evaluation based on elastic-plastic-creep analysis. *Journal of Electronic Packaging*, vol. 122, pp. 255-261.

Qian, Z.; Liu, S. (1999): On the life prediction and accelerated testing of solder joints. *The International Journal of Microcircuits and Electronic Packaging*, vol. 22, pp. 288-304.

Sanchez-Palencia, E. (1980): Non-homogeneous media and vibration theory. *Lecture Notes in Physics*, #127, Springer-Verlag, Berlin.

Solomn, H. D. (1986): Fatigue of 60/40 solder. *IEEE Transactions on Components, Hybrids, and Manufacturing Technology*, pp. 423-431.

Willis, J. R. (1977): Bound and self-consistent estimates for the overall properties of anisotropic composites. *Journal of the Mechanics and Physics of Solids*, vol. 25, pp. 185-202.

Zhang, X. W.; Lee S. W. R. (1998): Effect of temperature profile on the life prediction of PBGA solder joints under thermal cycling. *Key Engineer Materials*, vol. 145-149, pp. 1133-1138.

Appendix A: Moiré Interferometry

Moiré interferometry is a high sensitive optical technique for measuring the whole-field in-plane displacements. It is widely applied to investigate the thermal-mechanical behaviors of electronic packages in literature [Han and Guo (1995), Ham and Lee (2003)]. This study employs the technique to validate the validity of the proposed FE models.

The moiré interferometry system consists of an illumination system, a moiré interferometer and a camera system. The illumination system is composed of a coherent light, beam expander and collimator. The coherent light is a He-Ne source laser, with a wavelength of 632.8 nanometers. By adopting the illumination system, the coherent light is divided into four coherent beams, and two of which are for horizontal beams and the other two of which are for vertical beams. The separated beams are then directed onto the specimen, and then create a fringe pattern. When the two horizontal beams interfere, a horizontal deformation field is generated, which is called the U-field. In other words, the V-field is a vertical deformation field when the two vertical beams interfere. Finally, the fringes pattern is recorded as an image by utilizing the camera system for further analyses. Fig. 19 describes the schematic plot of the moiré interferometry system. Note that Fig. 19 only shows the two horizontal beams.

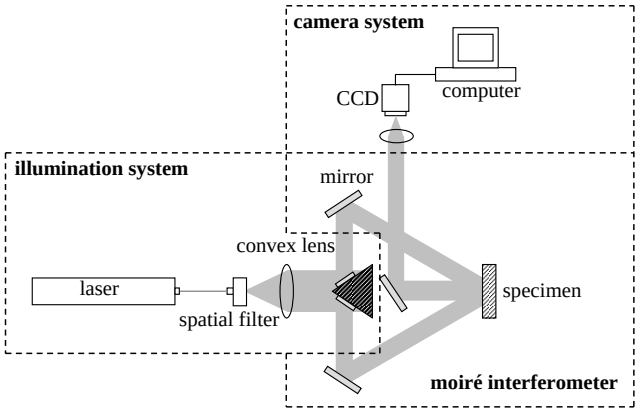

Figure 19 : Schematic diagram of the moiré interferometry system (Only two horizontal beams are shown)

According to the fringe pattern, the in-plane deformation of the specimen can be derived. The relationship between fringe order and displacement is expressed as follows:

$$U(x,y) = \frac{N_x(x,y)}{f_v} \tag{11}$$

$$V(x,y) = \frac{N_y(x,y)}{f_v} \tag{12}$$

where $U(x,y)$ and $V(x,y)$ are the relative displacement based on an arbitrarily selected reference point, $N_x(x,y)$ and $N_y(x,y)$ are the fringe order in the U-field and V-field, respectively, f_v is the frequency of the virtual reference grating.